metals

MDPI

Article

Phase Equilibrium and Austenite Decomposition in Advanced High-Strength Medium-Mn Bainitic Steels

Adam Grajcar [1,*], Władysław Zalecki [2], Wojciech Burian [2] and Aleksandra Kozłowska [1]

[1] Faculty of Mechanical Engineering, Silesian University of Technology, 18a Konarskiego Street, Gliwice 44-100, Poland; aleksandra.kozlowska@polsl.pl

[2] Institute for Ferrous Metallurgy, 12-14 K. Miarki Street, Gliwice 44-100, Poland; wzalecki@imz.pl (W.Z.); wburian@imz.pl (W.B.)

* Correspondence: adam.grajcar@polsl.pl; Tel.: +48-32-237-2940

Academic Editor: Carlos Garcia-Mateo

Received: 15 September 2016; Accepted: 14 October 2016; Published: 20 October 2016

Abstract: The work addresses the phase equilibrium analysis and austenite decomposition of two Nb-microalloyed medium-Mn steels containing 3% and 5% Mn. The pseudobinary Fe-C diagrams of the steels were calculated using Thermo-Calc. Thermodynamic calculations of the volume fraction evolution of microstructural constituents vs. temperature were carried out. The study comprised the determination of the time-temperature-transformation (TTT) diagrams and continuous cooling transformation (CCT) diagrams of the investigated steels. The diagrams were used to determine continuous and isothermal cooling paths suitable for production of bainite-based steels. It was found that the various Mn content strongly influences the hardenability of the steels and hence the austenite decomposition during cooling. The knowledge of CCT diagrams and the analysis of experimental dilatometric curves enabled to produce bainite-austenite mixtures in the thermomechanical simulator. Light microscopy (LM), scanning electron microscopy (SEM), and transmission electron microscopy (TEM) were used to assess the effect of heat treatment on morphological details of produced multiphase microstructures.

Keywords: medium-Mn steel; austenite decomposition; dilatometry; phase equilibrium; retained austenite

1. Introduction

The beneficial combination of high strength, ductility, and formability of steel sheets for the automotive industry can be achieved using advanced high-strength steels (AHSS). They consist of different soft and hard structural constituents in various proportions, which enable the attainment of a very wide range of mechanical and technological properties. The microstructure of dual-phase (DP) steel consists of soft ferrite and hard martensite, whereas the multiphase microstructure of TRIP (transformation-induced plasticity) steel comprises ferrite, bainite, and retained austenite [1–6]. New demands of the automotive industry for relatively low-cost steel sheets characterized by tensile strength above 1000 MPa require further searching for new chemical composition strategies. Advanced ultrahigh strength steels contain a higher fraction of hard phases (i.e., acicular ferrite, bainite, or martensite [7–10]) compared to AHSS containing polygonal ferrite as a matrix.

A key microstructural constituent of advanced multiphase steels is retained austenite in amounts from 10% to 30%. The latter phase ensures a required ductility level by its strain-induced martensitic transformation during cold-forming operations. Recently, a high amount of retained austenite can be obtained in different bainitic alloys containing from 1.5 to 8 wt. % of Mn, which is a main austenite stabilizer [8–14]. These steels are dedicated to the automotive industry for different crash-relevant

elements, especially in the side zone of a car (B-pillars, roof rails, side-impact beams, etc.). However, their wide use requires improvement of forming technologies and special welding procedures.

Monitoring the phase transformations and the knowledge of continuous cooling transformation (CCT) diagrams are of primary importance for proper design of bainite-austenite microstructures in medium-Mn steels. Austenite decomposition upon heating or during cooling from the γ region is often monitored by dilatometry, differential thermal analysis (DTA), or differential scanning calorimetry (DSC) [11,15–17]. Results of these investigations have to be confirmed by detailed microscopic research because phase transformations in multiphase steels are very complex. In medium-Mn steels, the bainite is particularly difficult for unequivocal identification because it can contain carbides or may form carbide-free bainite [8,18–22]. Films of retained austenite, instead of carbides, occur between laths of bainitic ferrite.

The destabilization of the austenite occurs during heating or cooling as a result of precipitation of carbides, martensitic transformation, and so forth. Monitoring the volume fraction of all microstructural constituents and their morphology is key to obtaining optimal mechanical properties of multiphase steels. Beneficial mechanical properties and formability of steels with a bainitic-austenitic mixture are obtained for fine, homogeneous bainite microstructures. Carbide precipitates and a bimodal morphology of fine and coarse bainite are detrimental for fracture toughness and ductility of steel products [19,20,23]. Thus, silicon or aluminum strategies are employed to avoid carbide precipitation during isothermal bainitic transformation step [24–27].

2. Materials and Methods

2.1. Materials

Medium-Mn steels contain from 3% to 12% of Mn. Steel with higher Mn contents are used mainly for cold-rolled products [3,10,12], but the steels relevant to the current study were being designed for hot-rolled products. Hence, the steels contained the lower levels of Mn (i.e., in a range from 3 to 5 wt. %). The carbon content in both steels was at a level of 0.17 wt. % (Table 1), which provides moderate hardenability. Aluminium concept was chosen to prevent carbide precipitation. Mo and Nb were added for solid solution hardening and precipitation strengthening. The alloys differed only in the manganese content, thus they were coded as 3 Mn and 5 Mn steels. The laboratory ingots, after vacuum induction melting, were hot-forged to obtain flat samples with a thickness of 22 mm. Cylindrical (solid) samples of $\phi 5 \times 7$ mm for dilatometric tests and cuboid samples of $15 \times 20 \times 35$ mm^3 for multistep compression tests were machined.

Table 1. Chemical compositions of the investigated medium-Mn steels.

Species	Grade								
	C %	Mn %	Al %	Si %	Mo %	Nb %	P %	S %	N %
3 Mn	0.17	3.1	1.6	0.22	0.22	0.04	0.008	0.005	0.0046
5 Mn	0.17	5.0	1.5	0.21	0.20	0.03	0.008	0.005	0.0054

2.2. Thermodynamic Calculations

The investigated steels belong to a new group of unconventional iron alloys due to untypical additions of Mn and Al. Hence, the precise selection of heat treatment or thermomechanical-processing conditions requires earlier thermodynamic calculations of phase compositions and other parameters. The first step required determination of pseudobinary iron-carbon systems for the investigated alloys using the Thermo-Calc package. The calculations of phase diagrams were performed by means of Thermo-Calc software using TCFE6 and SSOL2 databases [28]. The untypical alloying additions can substantially affect the decomposition of austenite upon cooling [29]. Thus, the time-temperature-transformation (TTT) diagrams for isothermal cooling conditions and continuous

cooling transformation (CCT) diagrams were calculated using the JMatPro (Sente Software Ltd., Guildford, UK) software [30]. This package was also used to monitor the evolution of potential phases as a function of temperature.

2.3. Experimental

The correctness of thermodynamic calculations was checked by dilatometric analysis and microstructure studies. Critical temperatures were determined using tubular samples of $\phi 4 \times \phi 2 \times 7$ mm, by means of a DIL805A/D dilatometer manufactured by Bähr Thermoanalyse GmbH (Hüllhorst, Germany). The solid samples of $\phi 5 \times 7$ mm in the dilatometric tests with deformation were heated under vacuum conditions (vacuum $< 10^{-4}$ mbar) to 1100 °C at a rate of 3 °C/s. After 300 s soaking at this temperature they were cooled to 900 °C at a rate of 5 °C/s. The holding time before deformation and subsequent cooling was 20 s. Then the samples were compressed, applying the true strain of 0.5 at a strain rate of 1/s. The continuous cooling rates to room temperature were selected as 0.5, 1, and 4 °C/s.

The final stage of the experimental study comprised the simulation of hot-working and cooling conditions used for production of thermomechanically processed TRIP steels with retained austenite. These conditions were reconstructed in the Gleeble 3800 thermomechanical simulator (Dynamic Systems Inc., Poestenkill, NY, USA). The initial processing schedule included resistance-heating of cubicoid samples to 1200 °C and their soaking within 30 s. Then, the samples were deformed using seven compression steps, summarized in Table 2. After the final deformation at 850 °C, the specimens were controlled cooled to room temperature to produce different multiphase microstructures. Since the decomposition of austenite substantially affects CCT and TTT diagrams, the cooling conditions will be presented in the next section after analysing phase transformations of undercooled austenite.

Table 2. Hot-working conditions.

Compression Step	Deformation Temperature, °C	True Strain	Strain Rate, s^{-1}	Time between Compression Steps, s
1	1150	0.4	5	30
2	1000	0.3	5	10
3	950	0.2	10	10
4	900	0.2	10	3
5	870	0.2	30	3
6	860	0.2	50	1
7	850	0.2	50	–

Light microscopy (LM), scanning electron microscopy (SEM), and transmission electron microscopy (TEM) were employed to identify phase composition of the investigated steels. Standard techniques for the preparation of metallographic samples were applied. Nital etching was used for dilatometric specimens whereas etching in 10% aqueous solution of sodium metabisulphite was applied to reveal retained austenite in thermomechanically processed samples. Morphological details of the microstructure were revealed with the SUPRA 25 SEM (Carl Zeiss, Jena, Germany). The quantitative metallography has been applied to determine the amount of ferrite fraction in dilatometric specimens. The presence of potential precipitations and substructure morphology were identified using JEOL JEM 2000 FX (JEOL USA, Inc., Peabody, MA, USA) electron microscope at an accelerating voltage of 160 kV.

3. Results and Discussion

3.1. Thermodynamic Calculations

The pseudobinary Fe-C phase diagram of 3 Mn steel determined using the Thermo-Calc is shown in Figure 1. It is clearly seen that the shape of the diagram in the high-temperature region is far from typical low-alloyed steels. The solidification of the alloy begins with crystallization of δ ferrite

from the liquid. The high addition of Al increased a maximum solubility of C in the δ ferrite to ca. 0.17 wt. %, corresponding to its content in the alloy. It is also obvious that for steels containing below 0.3 wt. % C, the stability of pure austenite cannot be obtained after passing through the two-phase region. Instead, the stability of austenite and ferrite occurs up to a eutectoid reaction at about 700 °C. This phenomenon is caused by the addition high amounts of Al, which is a strong ferrite former. Precipitation of niobium carbides starts to take place at a temperature of about 1200 °C under conditions of thermodynamic equilibrium.

The addition of 5 wt. % Mn slightly changes the pseudobinary Fe-C phase diagram, which is presented in Figure 2. As a result of the higher Mn addition, the solubility of C in δ ferrite decreased to approx. 0.12 wt. %. This means that some fraction of γ phase should be formed from the liquid. Manganese also shifts the two-phase region of γ + α to the left, but pure austenite still cannot be produced due to the opposite effect of Al. A temperature of equilibrium cementite precipitation decreased below 700 °C.

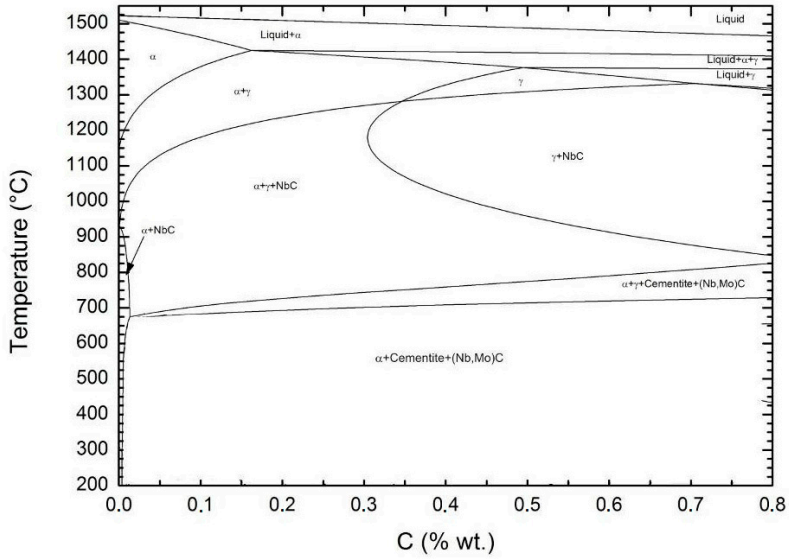

Figure 1. Pseudobinary Fe-C phase diagram of 3 Mn steel determined using Thermo-Calc.

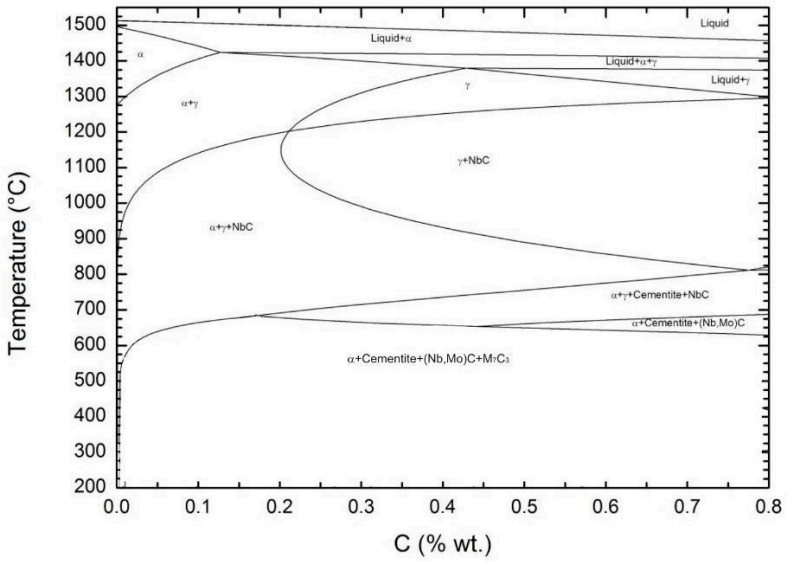

Figure 2. Pseudobinary Fe-C phase diagram of 5 Mn steel determined using Thermo-Calc.

Further details of the microstructure evolution as a function of temperature under equilibrium conditions can be assessed on the basis of Figures 3 and 4. Figure 3 shows the evolution of the potential structural constituents in the steel containing 3 wt. % of Mn. One can see that the solidification process is accompanied by precipitation of manganese sulphides. However, their amount should be relatively small, taking into account the high metallurgical cleanliness of the steels, as sulphur contents do not exceed the limit of ca. 0.005% (Table 1).

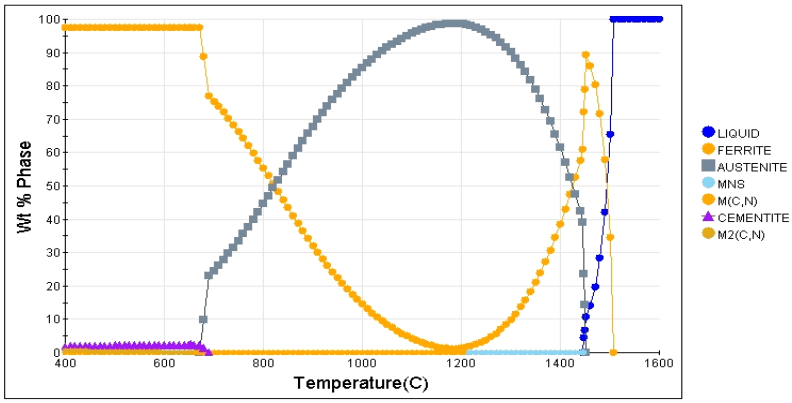

Figure 3. Equilibrium evolution of phases in 3 Mn steel calculated using the JMatPro package.

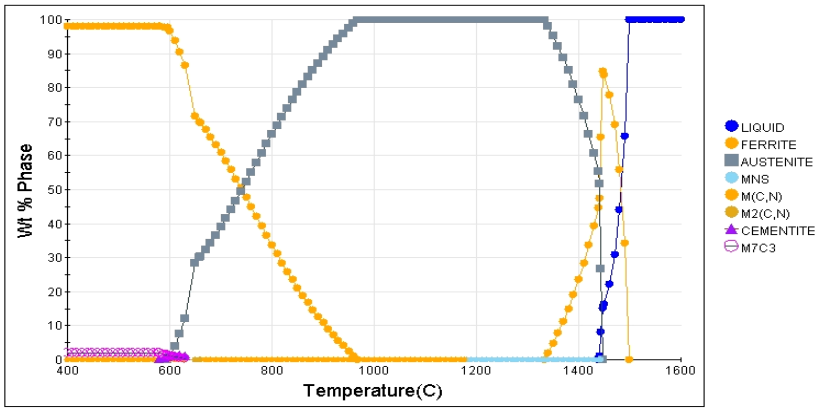

Figure 4. Equilibrium evolution of phases in 5 Mn steel calculated using the JMatPro package.

Figure 3 confirms the prediction of the pseudobinary Fe-C system of the 3 Mn steel concerning a lack of stable single γ phase. The maximum content of austenite with a small fraction of ferrite occurs under the equilibrium at a temperature of ca. 1180 °C. The α phase amount increases with the temperature drop. Below the eutectoid reaction cementite will be formed. The potential presence of M(C,N) and/or M_2(C,N) precipitates cannot be excluded.

The higher discrepancy between the Fe-C system (Figure 2) and the evolution of predicted phases occurs for the 5 Mn steel. Figure 4 suggests that there is a stable austenite field in a temperature range from ca. 1320–960 °C. On the other hand, Figure 2 does not contain the stable austenite region. However, it should be noted that for the C content of 0.17 wt. % this line is situated close to the transition line (γ + NbC). It seems that for new chemical compositions further improvements in Thermo-Calc and JMatPro packages are needed to predict more correctly the phase transitions of such complex systems. This especially concerns the combined effects caused by increased Mn and Al contents. These predictions have been validated partially in dilatometric tests performed, including plastic deformation of austenite at 900 °C prior to cooling. The results of these tests will be presented in Section 3.2. Further experiments are planned for long holding times at higher austenitizing temperatures followed by sample quenching to correlate the real phase state with equilibrium predictions.

Industrial technology development requires investigation of the microstructure evolution as a function of time. Thus, Figures 5 and 6 present predicted time-temperature-transformation (TTT) diagrams for both steels. The A_{e3} and A_{e1} temperatures are equal to 964 and 694 °C, respectively, for the 3 Mn steel, and they are substantially smaller for the steel containing 5 wt. % Mn: A_{e3} = 874 °C and A_{e1} = 655 °C. The evident effect of the high-Mn contents on the displacement of all phase transformations to a longer time is visible. This effect is especially significant for diffusion-controlled transformations. For example, the ferrite transformation begins after 100 s at 800 °C (Figure 5). In the case of the 5 Mn steel, the delay for the same isothermal holding temperature at which the ferrite is formed is even 10 times longer (Figure 6). It appears that the substantial hardenability effect of Mn suppresses the production of ferrite-based structures after cooling from an austenitization temperature.

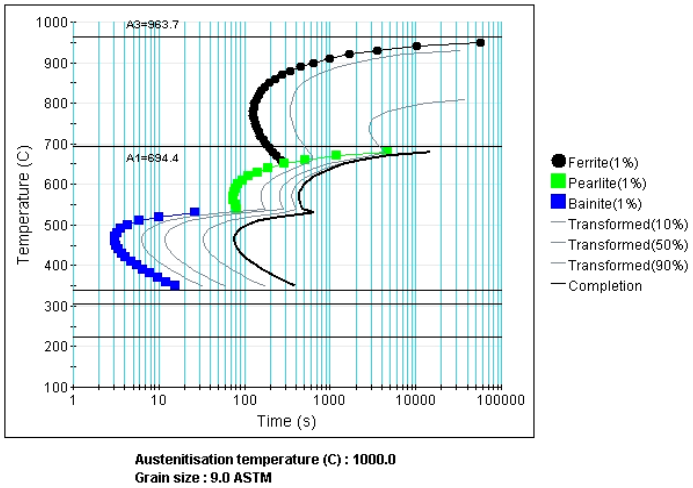

Figure 5. Predicted time-temperature-transformation (TTT) diagram of 3 Mn steel determined using the JMatPro package.

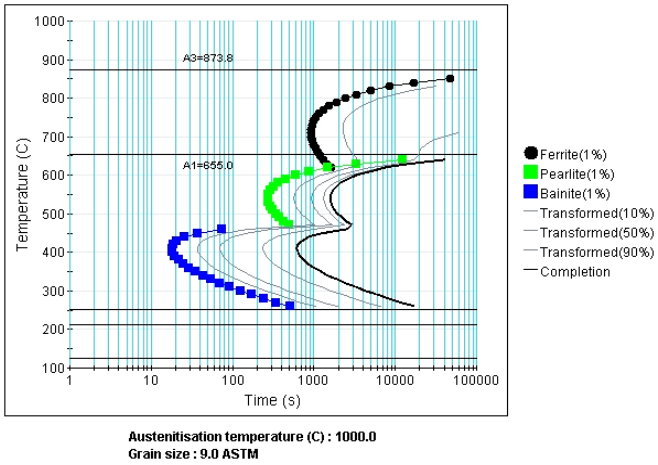

Figure 6. Predicted TTT diagram of 5 Mn steel determined using the JMatPro package.

It should be noted that both for isothermal and continuous cooling conditions, TTT and CCT diagrams are dependent on prior austenite grain size. For the present calculations the initial grain size of 9 ASTM (American Society for Testing and Materials, ASTM International) has been taken, which corresponds to a size of ca. 14 μm. An austenitizing temperature of 1000 °C has been assumed. The selected temperature and grain size may seem to be too low. However, the aim was to take into account a grain size after plastic deformation, which is usually successfully decreased during multistep deformation tests [21,24].

The pearlite transformation starts after ca. 70 s and 250 s at 560 °C, respectively, for the 3 Mn and 5 Mn steels. This delay is beneficial in terms of the production of carbide-free microstructures. The martensite start temperatures are relatively low: 340 °C for the 3 Mn steel and 251 °C for the alloy with the higher Mn content. The most interesting are bainitic bays in both steels because they constitute large technological temperature-time windows for realization of isothermal bainitic treatments, which are needed for production of carbide-free bainite-austenite mixtures [7,8,27].

A very similar situation is observed in the case of the continuous cooling transformation (CCT) diagrams (Figures 7 and 8). All regions of supercooled austenite transformations are shifted to the right. The displacement of ferrite allows supposition that it will be difficult to induce some fraction of this phase in hot-rolled sheets. This assumption has been confirmed in our earlier initial tests involving real dilatometric tests, which enabled the construction of experimental CCT diagrams [31]. The calculated and real CCT diagrams are in good agreement. However, further work is intended to explain in detail the presence of different phases, the effect of strain, composition, and cooling rates.

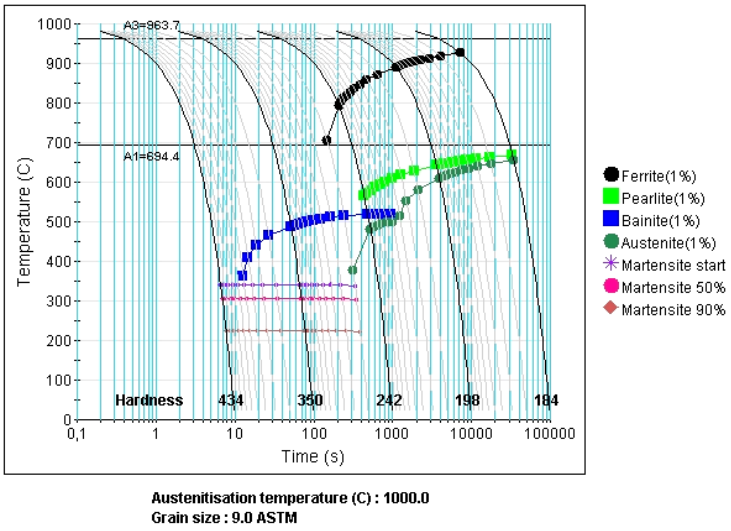

Figure 7. Predicted continuous cooling transformation (CCT) diagram of 3 Mn steel determined using the JMatPro package.

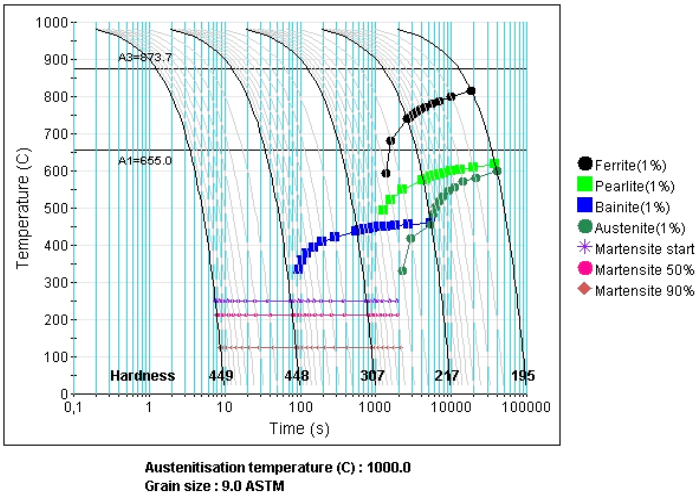

Figure 8. Predicted CCT diagram of 5 Mn steel determined using the JMatPro package.

It should be taken into account that plastic deformation shifts diffusion-controlled transformations to a shorter time [31,32]. JMatPro software does not enable the user to take into account the influence

of inner energy increase due to plastic deformation on phase transformations. Only a change of grain size may be applied. However, it requires some extra investigation of rheology of the material to gain reliable data. Thus, this behaviour requires experimental verification both in terms of ferrite production and carbide-free bainite formation.

The formation of bainite from the strained austenite is more complex compared to the ferrite transformation. The reason for that is a critical temperature region of bainitic transformation, at which diffusive and diffusionless transitions can take place. Moreover, the transformation behaviour strongly depends on a stress state. Bhadeshia [33] and Hase et al. [34] showed that, on the one hand, compressive or tensile stresses increase the bainite start temperature and the resulting transformation rate. On the other hand, the hydrostatic compression decreases the bainite formation rate. Considering the similarity of the bainitic transformation and martensite formation (in a low-temperature bainitic region) one can expect that deformation debris in the austenite retards the growth of bainite, causing a reduction in the fraction of transformation in spite of an increased number density of nucleation sites. This is called mechanical stabilization of bainite. At the same time, this phase is more refined [35]. Hence, the transformation rate is at first promoted by strain, and then it is retarded. This effect is stronger in a low-temperature range of bainitic transformation. Moreover, it should be noted that the austenite is usually inhomogeneously deformed. As a result, the lightly deformed regions transform rapidly because of the increase in the defect density, whereas the overall transformed area of the strongly deformed regions is smaller [33]. Finally, it results in bimodal distribution of bainite subunit sizes. The refinement of blocky austenite grains and the inherited increased dislocation density can support the stabilization of retained austenite within the bainitic matrix [12,35].

3.2. Dilatometric Tests

The representative dilatometric curves of the steel samples plastically deformed at 900 °C and then continuously cooled to room temperature at a rate of 1 °C/s are shown in Figures 9 and 10. Figure 9 presents dilatation changes for the steel containing the lower Mn content. Determination of ferrite start temperature is not easy because the deviation on the dilatometric curve is very small. Thus, developed in the Institute for Ferrous Metallurgy, a method of linear transformation of dilatometric curves was applied to get rid of "scale effect". The method of curve differentiation was also used, but the results were not good enough because of the scattering of experimental data. For the presented exemplary dilatometric curve in Figure 9, the phase composition comprised ca. 67% of bainite, 18% of martensite, and 15% of ferrite after applying a lever method. The A_{r3} temperature was determined to be 789 °C.

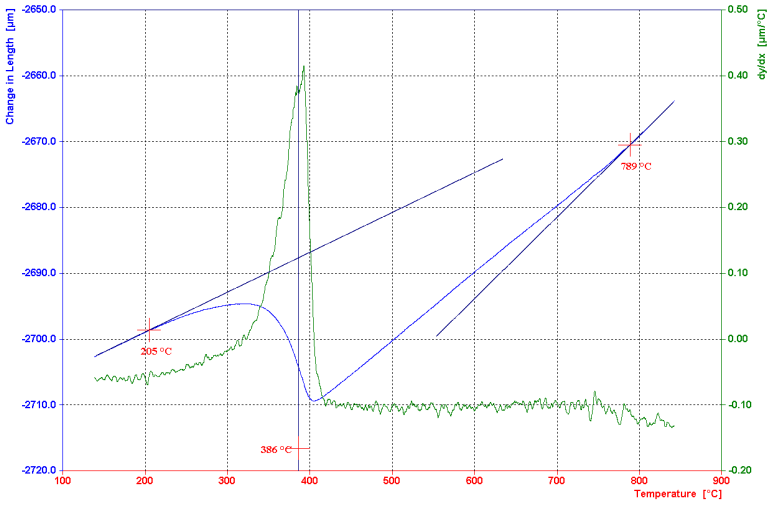

Figure 9. Dilatometric curve registered during cooling of 3 Mn steel at a rate of 1 °C/s.

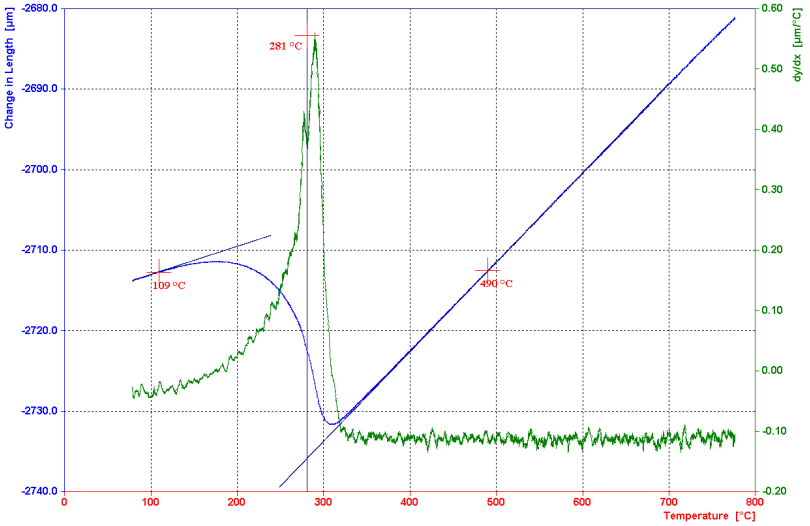

Figure 10. Dilatometric curve registered during cooling of 5 Mn steel at a rate of 1 °C/s.

The amount of austenite transformed into ferrite can be seen in Figure 11b. The average amount of ferrite—determined using an image analysis—contains 8.7% ± 1.6%, 8.5% ± 1.7%, and 2.3% ± 1.1%, respectively for the cooling rates of 0.5 °C/s, 1 °C/s, and 4 °C/s. Moreover, it is difficult to distinguish between a product of the austenite transformation and primary ferrite. The occurrence of the latter one confirms the correctness of Thermo-Calc predictions in Figure 1. Moreover, the fraction of large primary ferrite grains does not exceed ca. 7%, which is in good agreement with Figure 3. The application of the slower cooling rate amounting to 0.5 °C/s does not result in the essential increase of a fraction of ferrite (Figure 11a). This phase is still embedded in the bainite-martensite matrix. For faster cooling rates, only primary ferrite exists together with bainitic-martensitic mixture (Figure 11c).

The analysis of the dilatometric curve of the 5 Mn steel is easier because of a lack of an expansion signal from ferrite (Figure 10). The detailed analysis allowed estimating the bainite start temperature as ca. 490 °C. The martensite start temperature determined using differentiation of the curve was equal to 269 °C. These temperatures are significantly lower compared to the 3 Mn steel, which should be ascribed to the hardenability effect of manganese. The corresponding micrographs for the cooling rates from 0.5 °C/s to 4 °C/s are presented in Figure 11d–f. It is clear that these are ferrite-free bainitic-martensitic microstructures with the amount of martensite, which increases with faster cooling rates. A lack of primary ferrite corresponds well with the JMatPro calculations in Figure 4 and indicates some discrepancy between the experiment and calculations concerning the pseudobinary Fe-C system (Figure 2).

3.3. Microstructure of Thermomechanically Processed Samples

The phase transition calculations and dilatometric tests were the basis for the construction of final cooling schedules after multistep compression tests (Table 2). The results of analysis of dilatometric tests have made it clear that the present medium-Mn steels are not prone to obtaining ferrite-based microstructures. Therefore, the main cooling paths were designed in terms of the production of bainite-based microstructures. It should be noted that the applied cooling rates and deformation patters were different when compared to the dilatometric tests, which was obvious in terms of the design of multistep hot-strip rolling schedules. However, some fundamental indications on the effects of plastic deformation and cooling conditions on the transformation behaviour have been known. The most important information gained is regarding the difficulties in production of polygonal ferrite. The detailed cooling schedules are listed in Table 3. The essential step for stabilization of retained austenite is isothermal holding of deformed specimens at 450 °C within 300 s, where an incomplete bainitic transformation phenomenon should take place [16,23,27].

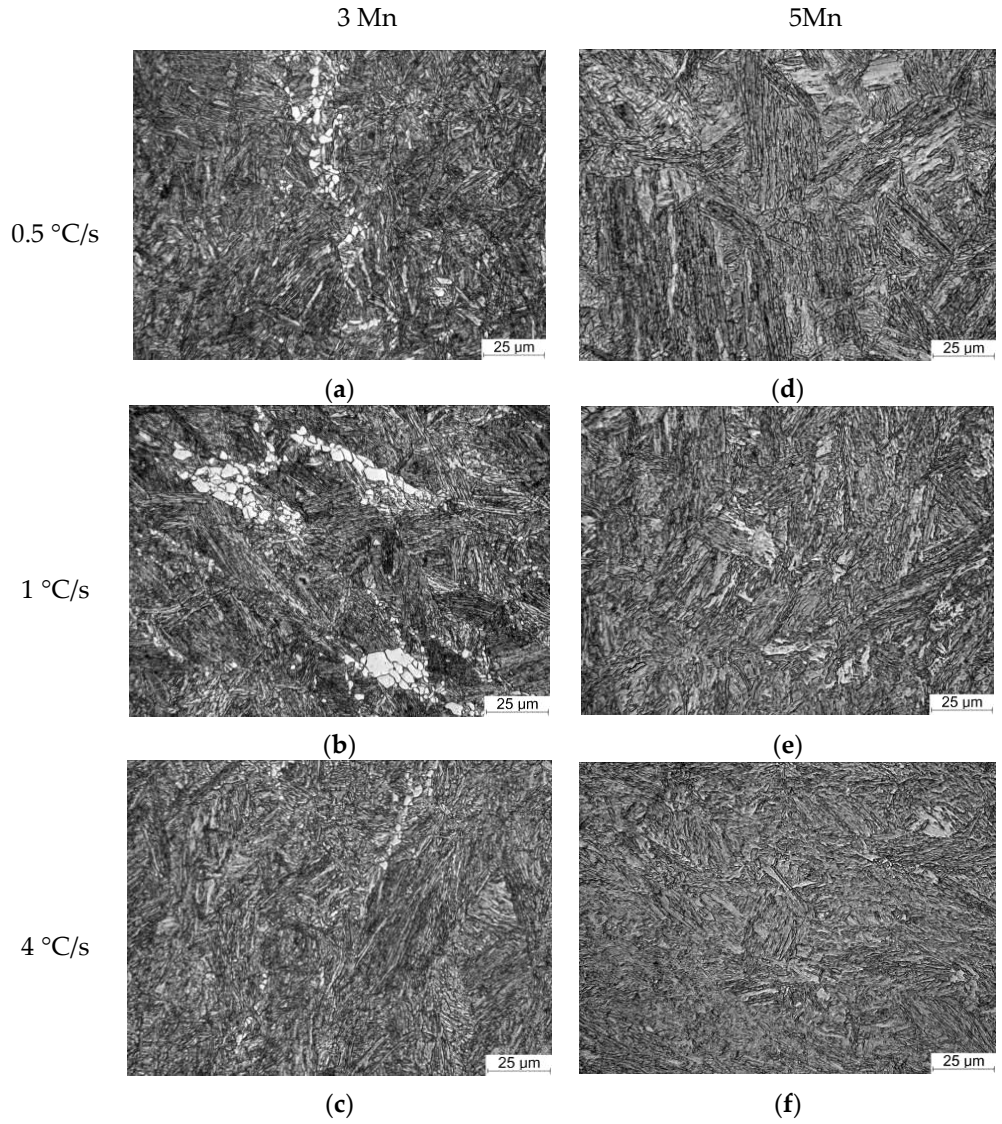

Figure 11. Microstructures obtained after deformation dilatometry tests for various cooling rates: (**a**,**d**) 0.5 °C/s; (**b**,**e**) 1 °C/s; (**c**,**f**) 4 °C/s.

Table 3. Cooling schedules following the multistep Gleeble simulations.

Temperature Range, °C	Cooling Rate, °C/s		
	3 Mn Steel Path 1	**3 Mn Steel Path 2**	**5 Mn Steel Path 3**
850 → 700 700 → 650 650 → 450	$V_1 = 30$ $V_2 = 5$ $V_3 = 40$	$V_1 = 30$	$V_1 = 30$
450	Isothermal holding at 450 °C within 300 s		
450 → RT	$V_4 = 0.5$	$V_2 = 0.5$	$V_2 = 0.5$
A Cooling Path	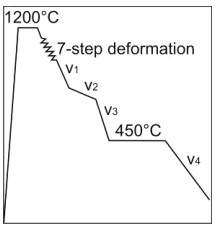	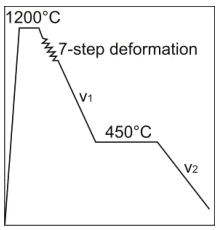	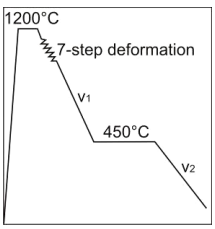

Paths 2 and 3 cover simple heat treatments following the final deformation step at 850 °C. Taking into account that plastic deformation accelerates ferrite transformation [31] and that the accumulative strain after seven-step compression is larger compared to the single-step deformation (realized in the dilatometer), we also designed Path 1 (Table 3). The aim of this test was to check if the severe multistep deformation (compared to dilatometer conditions) will induce ferrite in the 3 Mn steel or not. Thus, the essential step of Schedule 1 was cooling in a 700–650 °C temperature range at a relatively slow rate (5 °C/s). This temperature range corresponds to the ferrite bay of the steel in the CCT diagram (Figure 7).

The LM and SEM micrographs after the isothermal heat treatments according to the cooling Paths 1–3 are shown in Figure 12. Firstly, it is obvious that the multistep deformation results in the advanced grain refinement of the microstructure when compared to the dilatometric specimens. It concerns both granular and lathlike structural components. The LM micrographs are not sensitive enough to distinguish individual phases due to the small size of the constituents. The only clear conclusion is that the microstructures do not contain polygonal ferrite (Figure 12a–c). The slow cooling according to the Path 1 did not induce ferrite, and the main structural constituent is carbide-free bainite of bimodal granular and lath morphology (Figure 12d). A lack of carbide leads to the enrichment of austenite in carbon, and finally its presence at room temperature. In Figure 12d this phase can be observed as bright granules (RA) embedded inside the bainitic constituents. The amount of retained austenite is smaller for the 3 Mn steel cooled directly from 850 °C (Figure 12e). The γ phase is located between laths of bainitic ferrite. One can see that only interlath-retained austenite is stable whereas some blocky grains are partially transformed into martensite forming martensite-austenite (MA) constituents. The steel containing the higher Mn content shows univocal lath morphology (Figure 12f). Retained austenite is located within bainitic-martensitic mixture, but the amount of the γ phase is only minor. Kamoutsi et al. [10] reported that a smaller fraction of retained austenite is caused by the smaller driving force for the enrichment of austenite in carbon with increasing Mn content. A more detailed quantitative analysis of retained austenite is reported elsewhere [36].

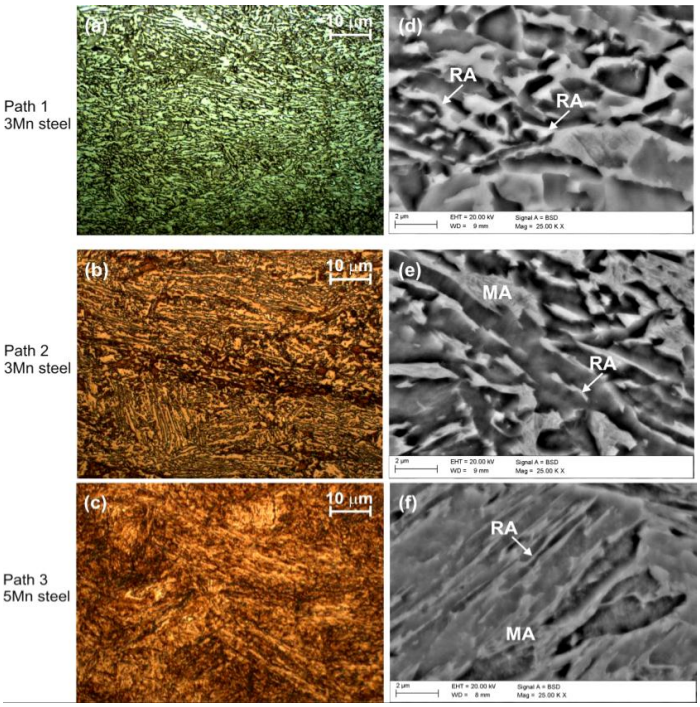

Figure 12. Multiphase bainite-based microstructures obtained after the thermomechanical treatment in the Gleeble simulator: (**a**–**c**) light microscopy (LM); (**d**–**f**) scanning electron microscopy (SEM); RA—retained austenite, MA—martensite-austenite constituents.

Morphological details of the microstructure have been assessed using transmission electron micrographs. Figure 13a shows a few granules of retained austenite within the granular bainite of relatively high dislocation density. The dislocations are a result of plastic deformation; however, some amount of them annihilates during slow cooling between 700 °C and 650 °C. The dislocation density increases for directly cooled samples because recovery processes are limited at 450 °C. Interlath-retained austenite of various thicknesses can be seen in Figure 13b. One can also see some austenite grains transformed partially into martensite (MA constituents). The 5 Mn steel contains predominantly continuous or interrupted laths of retained austenite embedded between the bainitic ferrite of high dislocation density.

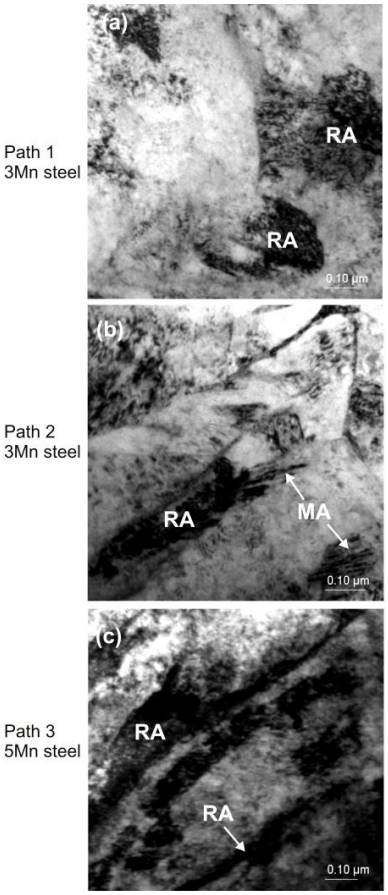

Figure 13. Transmission electron microscopy (TEM) micrographs showing the morphology of retained austenite and bainitic matrix in the: (**a**) 3 Mn steel (Path 1); (**b**) 3 Mn steel (Path 2); (**c**) 5 Mn steel (Path 3); RA—retained austenite, MA—martensite-austenite constituents.

The presence of possible MX phases (i.e., stable carbonitrides or carbides containing niobium) has not been revealed using a thin-film technique. Further experiments are in progress to confirm or negate this observation. However, our earlier investigations support the conclusion that there is a lack of MX carbides in the current medium-Mn steels. A reason for it is that the increase of Mn content increases the solubility of NbC and Nb(C,N) in the austenite and finally retards the precipitation of Nb(C,N) particles [36]. This effect is enhanced in steels containing a high content of Al fixing all of the nitrogen content.

4. Conclusions

The phase equilibrium state and austenite decomposition were analysed in two thermomechanically processed medium-Mn steels containing increased aluminium content. The increase of Mn concentration

from 3% to 5% substantially affects the equilibrium conditions and austenite decomposition. Some discrepancies between the pseudobinary Fe-C diagrams and JMatPro calculations concerning a volume-fraction phase evolution were revealed. It especially concerns an interphase between the stable austenite and austenite + ferrite region during austenitization. These discrepancies are caused by untypical Al + Mn contents, which strongly affect a phase constitution. Real dilatometric tests confirmed a lack of ferrite in the steel containing 5% Mn and the occurrence of some small amounts of this phase in the 3 Mn steel.

The presented steels are prone to producing bainitic-martensitic mixtures during continuous cooling, even for relatively small cooling rates of 0.5 °C/s. The dominant structural constituent is bainite. The application of austempering allowed production of the fine-grained carbide-free bainitic mixtures with retained austenite. The higher fraction of interlath and blocky-type retained austenite was obtained in the 3 Mn steel, as a result of the hampering effect of Mn on the enrichment of austenite in carbon.

Acknowledgments: This work was financially supported with statutory funds of Faculty of Mechanical Engineering of Silesian University of Technology in 2016.

Author Contributions: A.G. conceived and designed the experiments and wrote the paper; W.Z. performed dilatometric experiments and analyzed the results; W.B. performed the equilibrium calculations; A.K. analyzed the data and reviewed the paper.

Conflicts of Interest: The authors declare no conflict of interest.

References

1. Gronostajski, Z.; Niechajowicz, A.; Polak, S. Prospects for the use of new-generation steels of the AHSS type for collision energy absorbing components. *Arch. Metall. Mater.* **2010**, *55*, 221–230.
2. Gibbs, P.J.; de Moor, E.; Merwin, M.J.; Clausen, B.; Speer, J.G.; Matlock, D.K. Austenite stability effects on tensile behavior of manganese-enriched-austenite transformation-induced plasticity steel. *Metall. Mater. Trans. A* **2011**, *42A*, 3691–3702. [CrossRef]
3. Rana, R.; Gibbs, P.J.; de Moor, E.; Speer, J.G.; Matlock, D.K. A composite modeling analysis of the deformation behavior of medium manganese steels. *Steel Res. Int.* **2015**, *86*, 1139–1150. [CrossRef]
4. Klancnik, G.; Medved, J.; Nagode, A.; Novak, G.; Petrovic, D.S. Influence of Mn on the solidification of Fe-Si-Al alloy for non-oriented electrical steel. *J. Therm. Anal. Calorim.* **2014**, *116*, 295–302. [CrossRef]
5. Wielgosz, E.; Kargul, T. Differential scanning calorimetry study of peritectic steel grades. *J. Therm. Anal. Calorim.* **2015**, *119*, 1547–1553. [CrossRef]
6. Grajcar, A.; Kuziak, R. Softening kinetics in Nb-microalloyed TRIP steels with increased Mn content. *Adv. Mater. Res.* **2011**, *314–316*, 119–122. [CrossRef]
7. Grajcar, A.; Zalecki, W.; Skrzypczyk, P.; Kilarski, A.; Kowalski, A.; Kołodziej, S. Dilatometric study of phase transformation in advanced high-strength bainitic steel. *J. Therm. Anal. Calorim.* **2014**, *118*, 739–748. [CrossRef]
8. Grajcar, A.; Radwanski, K.; Krzton, H. Microstructural analysis of a thermomechanically processed Si-Al TRIP steel characterized by EBSD and X-ray techniques. *Solid State Phenom.* **2013**, *203–204*, 34–37. [CrossRef]
9. Radwanski, K.; Wrozyna, A.; Kuziak, R. Role of the advanced microstructures characterization in modeling of mechanical properties of AHSS steels. *Mater. Sci. Eng. A* **2015**, *639*, 567–574. [CrossRef]
10. Kamoutsi, H.; Gioti, E.; Haidemenopoulos, G.N.; Cai, Z.; Ding, H. Kinetics of solute partitioning during intercritical annealing of a medium-Mn steel. *Metall. Mater. Trans. A* **2015**, *46*, 4841–4846. [CrossRef]
11. Sugimoto, K.; Tanino, H.; Kobayashi, J. Impact toughness of medium-Mn transformation-induced plasticity-aided steels. *Steel. Res. Int.* **2015**, *86*, 1151–1160. [CrossRef]
12. Lee, S.; Lee, K.; de Cooman, B.C. Observation of the TWIP + TRIP plasticity-enhancement mechanism in Al-added 6 wt. pct medium Mn steel. *Metall. Mater. Trans. A* **2015**, *46*, 2356–2363. [CrossRef]
13. Garcia-Mateo, C.; Sourmail, T.; Caballero, F.G.; Capdevila, C.; de Andrés, C.G. New approach for the bainite start temperature calculation in steels. *Mater. Sci. Technol.* **2005**, *21*, 934–940. [CrossRef]
14. Farahani, H.; Xu, W.; van der Zwaag, S. Prediction and validation of the austenite phase fraction upon intercritical annealing of medium Mn steels. *Metall. Mater. Trans. A* **2015**, *46A*, 4978–4985. [CrossRef]

15. Skolek, E.; Marciniak, S.; Świątnicki, W.A. Thermal stability of nanocrystalline structure in X37CrMoV5-1 steel. *Arch. Metall. Mater.* **2015**, *60*, 511–516.
16. Kokosza, A.; Pacyna, J. Formation of medium carbon TRIP steel microstructure during annealing in the intercritical temperature range. *Arch. Metall. Mater.* **2014**, *59*, 1017–1022. [CrossRef]
17. Jirkova, H.; Masek, B.; Wagner, M.F.X.; Langmajerova, D.; Kucerova, L.; Treml, R.; Kiener, D. Influence of metastable retained austenite on macro and micromechanical properties of steel processed by the Q&P process. *J. Alloy. Compd.* **2014**, *615*, S163–S168.
18. Mazancova, E.; Ruziak, I.; Schindler, I. Influence of rolling conditions and aging process on mechanical properties of high manganese steels. *Arch. Civ. Mech. Eng.* **2012**, *12*, 142–147. [CrossRef]
19. Steineder, K.; Schneider, R.; Krizan, D.; Beal, C.; Sommitsch, C. Comparative investigation of phase transformation behavior as a function of annealing temperature and cooling rate of two medium-Mn steels. *Steel Res. Int.* **2015**, *86*, 1179–1186. [CrossRef]
20. Mesquita, R.A.; Schneider, R.; Steineder, K.; Samek, L.; Arenholz, E. On the austenite stability of a new quality of twinning induced plasticity steel, exploring new ranges of Mn and C. *Metall. Mater. Trans A* **2013**, *44*, 4015–4019. [CrossRef]
21. Opiela, M. Thermomechanical treatment of Ti-Nb-V-B micro-alloyed steel forgings. *Mater. Tehnol.* **2014**, *48*, 587–591.
22. Lisiecki, A. Welding of thermomechanically rolled fine-grain steel by different types of lasers. *Arch. Metall. Mater.* **2014**, *59*, 1625–1631.
23. Bhadeshia, H.K.D.H. Anomalies in carbon concentration determinations from nanostructured bainite. *Mater. Sci. Technol.* **2015**, *31*, 758–763. [CrossRef]
24. Grajcar, A.; Lesz, S. Influence of Nb microaddition on a microstructure of low-alloyed steels with increased manganese content. *Mater. Sci. Forum* **2012**, *706–709*, 2124–2129. [CrossRef]
25. Kucerova, L.; Jirkova, H.; Masek, B. The effect of alloying on mechanical properties of advanced high strength steels. *Arch. Metall. Mater.* **2014**, *59*, 1189–1192.
26. Jablonska, M.; Smiglewicz, A. A study of mechanical properties of high manganese steels after different rolling conditions. *Metalurgija* **2015**, *54*, 619–622.
27. Zhao, L.; Top, K.A.; Rolin, V.; Sietsma, J.; Mertens, A.; Jacques, P.J.; van der Zwaag, S. Quantitative dilatometric analysis of intercritical annealing in a low-silicon TRIP steel. *J. Mater. Sci.* **2002**, *37*, 1585–1591. [CrossRef]
28. Thermo-Calc Software. Available online: http://www.thermocalc.com/products-services/databases/ (accessed on 3 October 2016).
29. Trzaska, J. Empirical formulae for the calculation of austenite supercooled transformation temperatures. *Arch. Metall. Mater.* **2015**, *60*, 181–185. [CrossRef]
30. Saunders, N.; Guo, Z.; Li, X.; Miodownik, A.P.; Schillé, J.P. Using JMatPro to model materials properties and behavior. *JOM* **2003**, *55*, 60–65. [CrossRef]
31. Grajcar, A.; Kuziak, R.; Zalecki, W. Third generation of AHSS with increased fraction of retained austenite for the automotive industry. *Arch. Civ. Mech. Eng.* **2012**, *12*, 334–341. [CrossRef]
32. Caballero, F.G.; Garcia-Mateo, C.; García de Andrés, C. Dilatometric study of reaustenitisation of high silicon bainitic steels: Decomposition of retained austenite. *Mater. Trans.* **2005**, *46*, 581–586. [CrossRef]
33. Bhadeshia, H.K.D.H. *Bainite in Steels. Transformations, Microstructure and Properties*, 2nd ed.; Institute of Materials, Minerals and Mining: London, UK, 2001; pp. 201–224.
34. Hase, K.; Garcia-Mateo, C.; Bhadeshia, H.K.D.H. Bainite formation influenced by large stress. *Mater. Sci. Technol.* **2004**, *20*, 1499–1505. [CrossRef]
35. Avishan, B.; Garcia-Mateo, C.; Morales-Rivas, L.; Yazdani, S.; Caballero, F.G. Strengthening and mechanical stability mechanisms in nanostructured bainite. *J. Mater. Sci.* **2013**, *48*, 6121–6132. [CrossRef]
36. Grajcar, A.; Skrzypczyk, P.; Kuziak, R.; Gołombek, K. Effect of finishing hot-working temperature on microstructure of thermomechanically processed Mn-Al multiphase steels. *Steel Res. Int.* **2014**, *85*, 1058–1069. [CrossRef]

© 2016 by the authors; licensee MDPI, Basel, Switzerland. This article is an open access article distributed under the terms and conditions of the Creative Commons Attribution (CC-BY) license (http://creativecommons.org/licenses/by/4.0/).